



**HAL**  
open science

## Intraseasonal rainfall variability over Madagascar

Clémence Macron, Yves Richard, Thomas Garot, Miloud Bessafi, Benjamin Pohl, Adolphe Ratiarison, Andrianaharimanana Razafindrabe

► **To cite this version:**

Clémence Macron, Yves Richard, Thomas Garot, Miloud Bessafi, Benjamin Pohl, et al.. Intraseasonal rainfall variability over Madagascar. *Monthly Weather Review*, 2016, 144 (5), pp.1877-1885. 10.1175/MWR-D-15-0077.1 . hal-01182564

**HAL Id: hal-01182564**

**<https://hal.science/hal-01182564>**

Submitted on 21 Nov 2020

**HAL** is a multi-disciplinary open access archive for the deposit and dissemination of scientific research documents, whether they are published or not. The documents may come from teaching and research institutions in France or abroad, or from public or private research centers.

L'archive ouverte pluridisciplinaire **HAL**, est destinée au dépôt et à la diffusion de documents scientifiques de niveau recherche, publiés ou non, émanant des établissements d'enseignement et de recherche français ou étrangers, des laboratoires publics ou privés.

## Intraseasonal Rainfall Variability over Madagascar

CLÉMENCE MACRON,\* YVES RICHARD,\* THOMAS GAROT,<sup>+</sup> MILOUD BESSAFI,<sup>#</sup> BENJAMIN POHL,\*  
ADOLPHE RATIARISON,<sup>@</sup> AND ANDRIANAHARIMANANA RAZAFINDRABE<sup>&</sup>

\* *Centre de Recherches de Climatologie, UMR6282 Biogéosciences, CNRS/Université de Bourgogne–Franche-Comté, Dijon, France*

<sup>+</sup> *LATMOS/IPSL, UVSQ Université Paris-Saclay, CNRS, Guyancourt, France*

<sup>#</sup> *Laboratoire d'Électronique, d'Énergétique et des Procédés, Université de la Réunion, Réunion, France*

<sup>@</sup> *Laboratoire de la Dynamique de l'Atmosphère du Climat et des Océans, Faculté des Sciences, Université d'Antananarivo, Antananarivo, Madagascar*

<sup>&</sup> *Laboratoire Hydraulique et énergétique, Ecole Supérieure Polytechnique, Université d'Antsirana, Antsirana, Madagascar*

(Manuscript received 3 March 2015, in final form 9 June 2015)

### ABSTRACT

Using daily rain gauge records for Madagascar and nearby islands, this paper investigates rainfall intraseasonal variability at local and regional scales during the austral summer season (November–February), as well as the respective influences of recurrent convective regimes over the southwest Indian Ocean (SWIO) and the Madden–Julian oscillation (MJO). The results show a general consistency between local-scale rainfall variability in Madagascar and regional-scale features of climate variability. The influence of tropical temperate troughs in their mature phase and/or their easternmost locations is first underlined. The development of such systems over southern Africa and the Mozambique Channel can be considered as precursors for Malagasy wet spells, especially over the southern part of the island. Regional and local effects of the MJO are weaker on average, and only concern the northwest of the island and the north of the Mozambique Channel. MJO and convective regimes are finally shown to explain distinct fractions of regional rainfall variability.

### 1. Introduction

Madagascar (592 040 km<sup>2</sup>) extends from 12° to 25°S in the southwest Indian Ocean (SWIO), about 500 km east off the eastern coast of southern Africa. Its marked topography mostly consists of coastal plains in the west, an inner plateau ending with abrupt edges in the east, and three major massifs inland: Tsaratanana (2876 m) in the north, and Ankaratra (2642 m) and Andringitra (2658 m) in the south (Fig. 1a). Such topography plays an important role on local weather and climate.

Madagascar is characterized by two contrasted seasons: a dry season from May to October and a wet season from November to April (Jury et al. 1995; Nassor and Jury 1997). Seasonal rainfall presents a very strong west–east gradient, with amounts 2 to 3 times larger on the east than on the west (Jury et al. 1995). In contrast, northern

Madagascar receives more rainfall on its western part due to mesoscale convective systems, tropical cyclones (TCs), depressions, and storms over the SWIO, and the northwest monsoon (Jury et al. 1995; Nassor and Jury 1998).

Despite the importance of rainfall in Madagascar where rain-fed agriculture supports 4 out of 5 people, few studies have focused on this region. This is probably due to the scarcity of in situ rainfall observations, especially at the daily time scale. Using an original dataset regrouping 30-yr-long daily rain gauge records over Madagascar (31 stations), the Réunion Island and Mayotte (1 station each), and 4 stations in the Scattered Islands (Europa, Juan Nova, Glorieuses, and Tromelin, Fig. 1a), this paper aims to contribute to fill this gap through an analysis of Malagasy rainfall intraseasonal variability. Its imbrication in regional or near-global climate variability is specifically investigated, particularly with tropical temperate troughs (TTTs), known as significant rain-producing systems over the southern African region (Todd and Washington 1999; Washington and Todd 1999; Fauchereau et al. 2009; Pohl et al. 2009).

Corresponding author address: Benjamin Pohl, Centre de Recherches de Climatologie, CNRS/Université de Bourgogne–Franche-Comté, 6 Bd. Gabriel, 21000 Dijon, France.  
E-mail: benjamin.pohl@u-bourgogne.fr

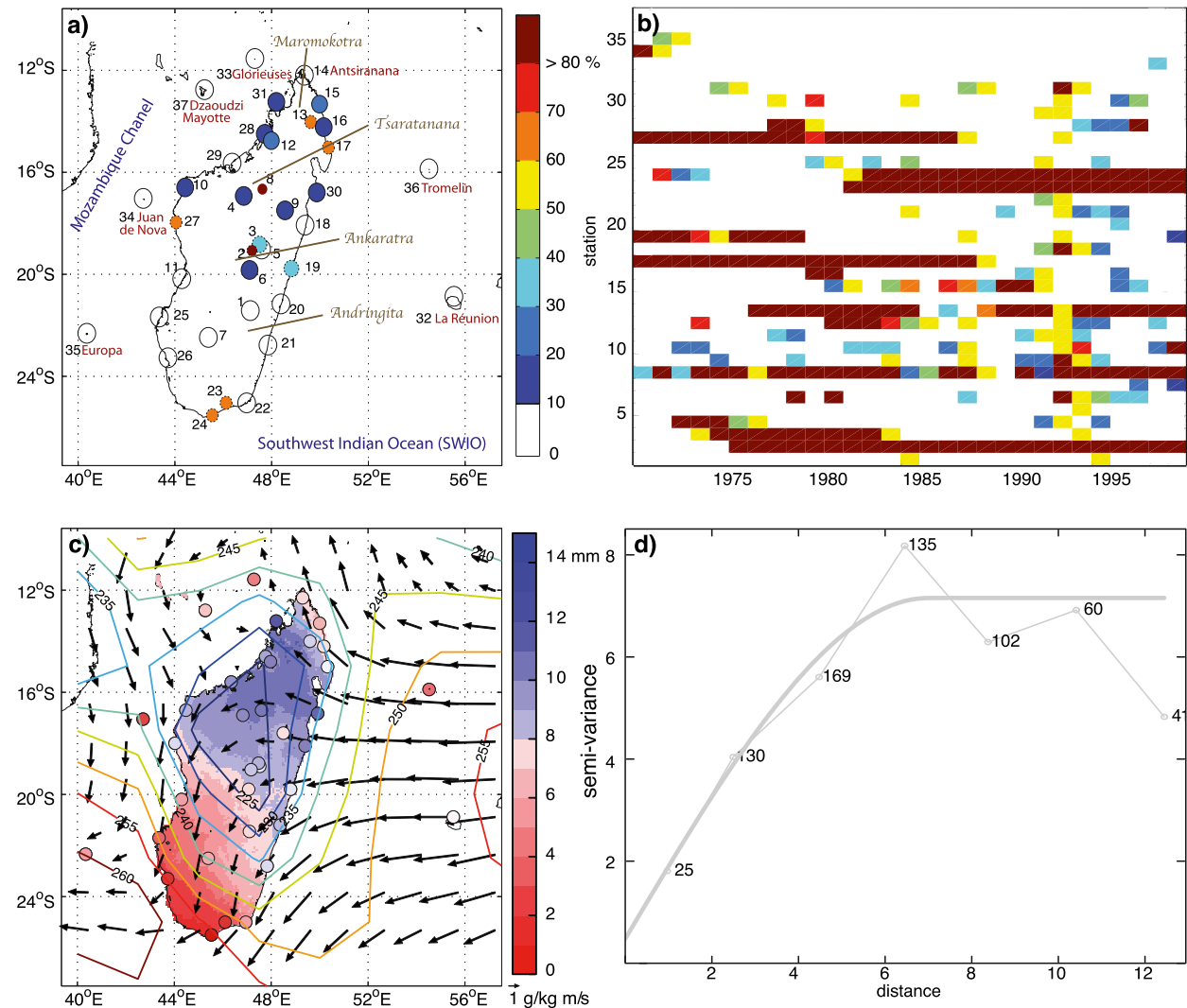


FIG. 1. (a) Location of the 37 daily rainfall stations and percentage of missing values. The dot size is proportional to the percentage of missing values (stations with fewer missing values are larger); the colors also represent the percentage of missing values (see color scale for legend). Names cited in the text appear in red for stations, in blue for ocean sectors, and in brown for mountains. (b) Temporal distribution of the missing values for each of the 37 stations for NDJF 1971–99. (c) Mean 1971–2000 seasonal rainfall for the austral summer season (NDJF) and for each station (circles), seasonal rainfall obtained with the RK methodology (shadings), and moisture fluxes integrated between 1000 and 700 hPa (vectors,  $g kg^{-1} m s^{-1}$ ). Contours show the seasonal mean OLR field ( $W m^{-2}$ ) during the same period. (d) Variogram of NDJF mean rainfall. Horizontal axis: distance in degrees, vertical axis: semivariance in  $mm day^{-1}$ . Solid line: semi-variance calculated for every 2°, from 1.5° to 15°. Thick line: spherical adjustment with nugget 0.5, sill 7.0, and range 6.0.

Another focus is on the Madden–Julian oscillation (MJO), the leading mode of intraseasonal variability in the tropics, which has nonnegligible impacts (i) on southern African rainfall and atmospheric convection variability (Pohl et al. 2007), and (ii) on tropical cyclones activity over the SWIO (Bessafi and Wheeler 2006). We discuss here its regional effects over the SWIO and its local signature in Madagascar.

To address the question of the relationships between Malagasy rainfall, TTT, and MJO, we propose to (i) document local rainfall variability associated with recurrent

convective regimes over the SWIO region such as calculated by Fauchereau et al. (2009), and the phases of the MJO, as depicted by the indices developed by Wheeler and Hendon (2004); (ii) infer to what extent such local rainfall variability may differ from large-scale convection estimates provided by global reanalyses and spatially interpolated rainfall structures derived from a regression-kriging procedure; and (iii) quantify to what extent regional convective regimes and the near-global MJO phases covary and may explain different fractions of local-scale rainfall variability.

This study is organized as follows. [Section 2](#) presents the datasets and the methodology used for this work. [Section 3](#) is devoted to the presentation of our results. Finally, [section 4](#) contains the conclusions and discussion.

## 2. Data and methods

### a. Observation and atmospheric data

This study concentrates on the summer rainfall season [November–February (NDJF)] for the period 1971–99. Daily rainfall amounts over Madagascar, Mayotte, La Réunion, and the Scattered Islands are provided by an original rain gauge database supplied by local universities, research organizations, and Météo-France. Although the network is not dense, stations are well distributed in space ([Fig. 1a](#)). A total of 28 stations (out of 37), presenting less than 30% of missing values, are extracted on the study period ([Fig. 1a](#)). Temporally ([Fig. 1b](#)), the missing values are not distributed homogeneously. Only five stations (14: Antsiranana; 32: La Réunion; 33: Glorieuses; 36: Tromelin; and 37: Dzaoudzi) present no missing values.

Large-scale atmospheric fields are documented by the 40-yr European Centre for Medium-Range Weather Forecasts (ECMWF) Re-Analysis (ERA-40; [Uppala et al. 2005](#)), in order to fit the study period for which rainfall observation is available. As in [Macron et al. \(2014\)](#), we make use of the daily outgoing long-wave radiation (OLR) over the period 1971–99 at a  $1.5^\circ \times 1.5^\circ$  spatial resolution as a proxy for deep convective activity. The reliability of this variable is also discussed in the same study (*ibid.*). Atmospheric variables (zonal  $U$  and meridional  $V$  components of the wind, and specific humidity) are derived from the same reanalyses.

### b. Composite analyses

Composite analyses are used to study rainfall and atmospheric circulation patterns associated with the MJO and recurrent convective regimes.

The MJO consists of large-scale deep convective anomalies, associated with lower- (upper) layer zonal wind convergence (divergence), that propagate from the Indian Ocean toward the Maritime Continent and the western Pacific, with a periodicity typically comprising between 30 and 60 days. Its dynamical and convective signal is monitored through the daily Real-time Multivariate MJO (RMM) indices developed by [Wheeler and Hendon \(2004\)](#). All moderate to strong MJO events are first selected, by extracting the days having an MJO amplitude greater than one standard deviation. We isolate next the days corresponding to

the eight different phases of the MJO. On average during the austral summer season, the MJO convective clusters initiate over the western Indian Ocean at phase 1, propagate eastward and reach the Maritime Continent of Indonesia at phases 4–5, and the western Pacific and the date line at phase 6; they next weaken over the Americas, the Atlantic basin, and tropical Africa.

The same composite approach is used at the regional scale using the recurrent convective regimes first discussed in [Fauchereau et al. \(2009\)](#), and also used in [Vigaud et al. \(2012\)](#) and [Macron et al. \(2014\)](#). They are obtained as the result of a clustering analysis [or  $k$ -means clustering; [Cheng and Wallace \(1993\)](#); [Michelangeli et al. \(1995\)](#)] of daily OLR anomalies over southern Africa and the SWIO. Following these previous studies, the optimal number of classes  $k$  to be retained is seven. The regimes were shown to be weakly sensitive to the input dataset (NOAA's satellite estimates derived from the AVHRR sensor or ERA-40's reanalyzed fields) as well as the period of analysis ([Macron et al. 2014](#)). To match the availability period of the rain gauge records, we use here ERA-40 daily fields during 1971–99.

### c. Geostatistical upscaling

Observed rainfall data are interpolated using a regression-kriging method (RK; [Odeh et al. 1995](#)). The RK method, mathematically equivalent to kriging with external drift (KED; [Hengl et al. 2007](#)), is suitable as a nonstationary model for mapping rainfall ([Lloyd 2010](#)). This method generally performs well in areas of complex topography (e.g., [Prudhomme and Reed 1999](#)). For further details, see [Hengl \(2009\)](#) and [Morel et al. \(2014\)](#).

First, a regression linear model (RLM) is used with three predictors: altitude, longitude, and latitude. For each rainfall pattern (seasonal mean or daily mean for each OLR regime or MJO phase), three simple and one multiple linear models are computed. The determination coefficients ( $r^2$ ) show that the role of altitude in rainfall spatial variability is very weak and never reaches the 95% significance level. Rainfall patterns are better described by trend surfaces; the retained combinations of altitude, longitude, and latitude only explain a small fraction of the total variance (e.g., 19.5% for seasonal rainfall). This suggests that the spatial sampling (i.e., the number of rain gauge stations) is not dense enough to accurately document the rainfall field, given the size of Madagascar and the complexity of its relief.

By considering that variation in the residual values of the RLM is distance dependent, spatial correlations can

next be used to improve local predictions. The experimental variograms (Fig. 1d) show clear spatial structures that fit well to a spherical model (Pebesma 2004). The semivariance converges toward an asymptote at about  $6^{\circ}$ – $8^{\circ}$ . This distance is defined as the range. The estimated semivariance at  $0^{\circ}$  is referred to as the nugget (here 0.4). The value at the range is referred to as the sill (here 7). With the sill strongly higher than the nugget and a well-identified range for samples with hundreds of values, we can statistically validate and confirm the robustness of the kriging procedure.

For seasonal rainfall (Fig. 1c), the mean error estimated through a leave-one-out cross validation is 0.11 mm and the standard deviation for the 28 rain gauges is 2.19 mm. The RK interpolation accurately highlights the well-known rainfall gradient prevailing over above 90% of Madagascar, with minimum (maximum) amounts located over the southwestern coasts (north of Madagascar over Mount Maromokotra). The impact of the RLM is prominent here. Thus, the map is smoother than those done with the Climate Hazards Group integrating infrared satellite data (CHIRPS) at a  $0.05^{\circ}$  resolution (Funk et al. 2014). Kriging the residuals also allows detecting smaller-scale features (that cannot exceed a distance of  $6^{\circ}$ ; Fig. 1c), such as rather dry conditions in the northeast. With as few stations containing missing data, it might be unwise to validate in detail this finescale structure, although the moisture fluxes seem to accredit it.

Rainfall, OLR, and moisture fluxes seasonal mean fields (Fig. 1c), mostly result from the presence of (i) the Mascarene high (or south Indian Ocean anticyclone) off the east coast, which favors moisture advections toward the eastern part of Madagascar throughout the year; and (ii) a monsoon circulation (in January and February) generating some moisture fluxes along the north and west coasts. These combined influences, modulated by the relief, result in moisture convergence over the central and northern mountains, where rainfall is abundant, and atmospheric convection is often active ( $225 \text{ W m}^{-2}$  on average). In the north and in the southern half of the island by contrast, moisture divergence and more stable atmospheric convection prevail ( $255 \text{ W m}^{-2}$  in the southern part of the island), together with much drier conditions.

### 3. Results

#### a. Regional convective regimes

Figure 2 shows the composite anomalies of OLR and moisture fluxes, vertically integrated between the surface and 700 hPa, during the seven convective regimes. Regimes 5, 6, and 7 (Figs. 2e–g) are characterized by

negative OLR anomalies (enhanced convection) associated with lower-layer moisture convergence, and forming a cloud band elongated along a northwest–southeast direction and linking the tropics ( $15^{\circ}\text{S}$ ) to the midlatitudes ( $45^{\circ}\text{S}$ ). These patterns are interpreted as synoptic-scale TTTs; the main difference between the three regimes is their longitudinal location, already discussed in previous work (Todd and Washington 1999; Washington and Todd 1999; Fauchereau et al. 2009; Pohl et al. 2009). Macron et al. (2014) recently pointed out that roughly 70% of TTT tend to propagate toward the east during their life cycle, hence, preferential transitions are from regimes 5–6 and 6–7. Other regimes (Figs. 2a–d) are solely related to tropical (temperate) anomalies for regimes 1–2–3 (regime 4). Based on such large-scale OLR anomalies, one can note that all seven regimes are likely to modulate daily rainfall over Madagascar, albeit weakly for regime 4.

To examine the possible disagreements between local-scale observations and larger-scale estimations, composite daily rainfall anomalies are next computed during the occurrences of the seven convective regimes (Fig. 2). Regimes 1 and 5 (regime 3) are associated with overall dry (wet) conditions over Madagascar and neighboring islands, consistent with the sign of the OLR anomalies in Figs. 2a and 2e (Fig. 2c). Dry conditions result from anticyclonic anomalies over the SWIO and/or southerly flux anomalies close to the islands associated with lower-layer divergence; generalized wet conditions are associated with moisture convergence close to Madagascar. For these regimes, local-scale measurements corroborate large-scale estimates, although a few stations do not present significant anomalies or even show weak, insignificant reverse sign signals. During the occurrences of regimes 2 and 6 (Figs. 2b,f) Malagasy rainfall fields show southwest–northeast (northeast–southwest) gradients, once again consistent with large-scale atmospheric configurations. These local gradients, respectively, attributed to strong cyclonic anomalies over the SWIO for regime 2, interpreted as a transient weakening of the Mascarene high and favoring moisture advections over the northern tip and the eastern part of Madagascar, and the presence of a TTT over the Mozambique Channel for regime 6, thus, enhancing convective activity southwest of Madagascar. For regime 7 the TTT reach their easternmost location, hence, the wet conditions in eastern Madagascar and the Mascarene Islands. As expected, regime 4 is associated with weak, barely significant anomalies; a few stations record significant dry anomalies, which did not appear in the large-scale fields.

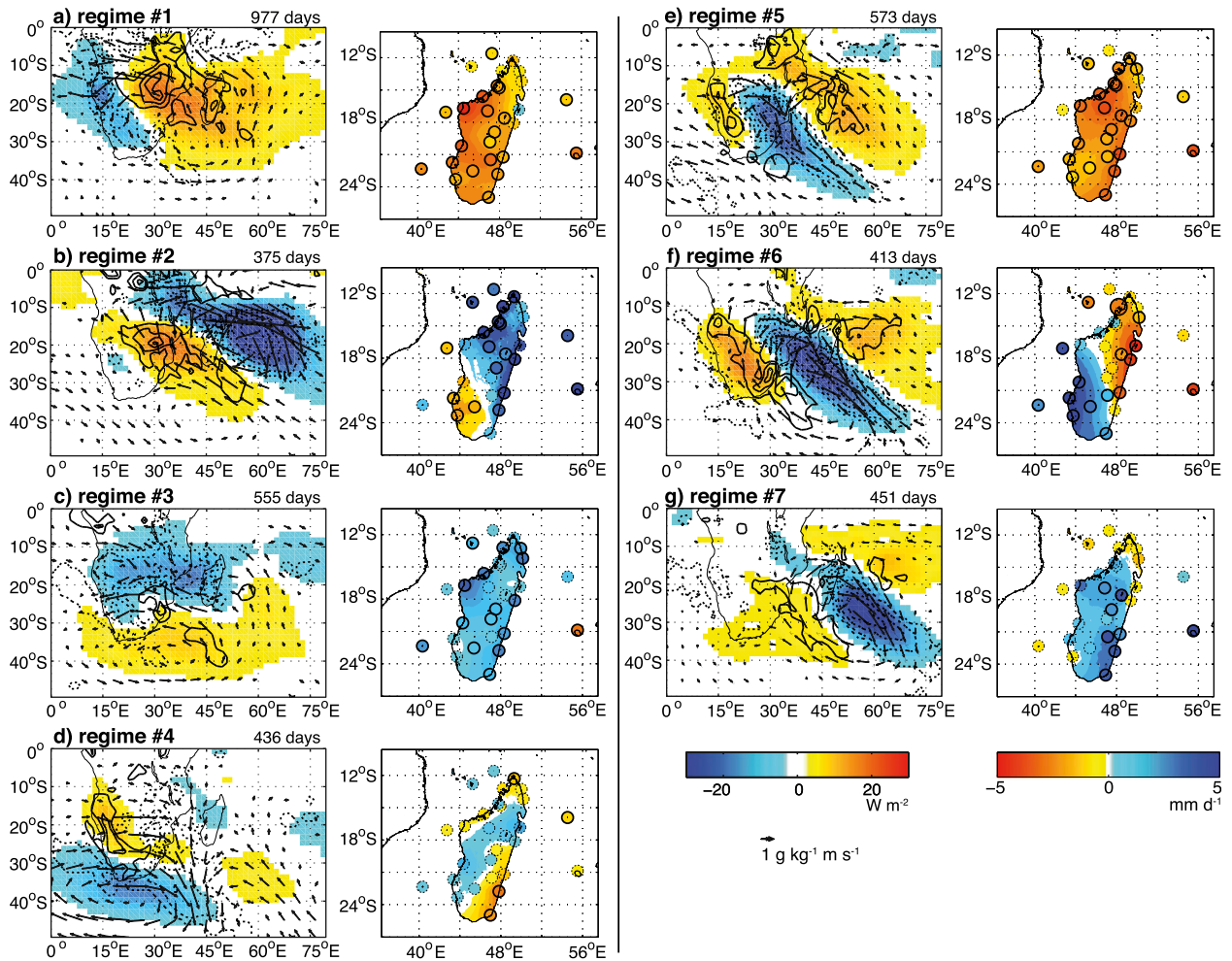


FIG. 2. Mean daily OLR anomalies (shadings,  $W m^{-2}$ ), moisture flux anomalies integrated between 1000 and 700 hPa (vectors;  $g kg^{-1} m s^{-1}$ ), and corresponding convergence (contours: solid curves for divergence, dashed curved for convergence;  $g kg^{-1} s^{-1}$ ) for the seven OLR regimes over the period NDJF 1971–99, and associated station rainfall anomalies. The negative (positive) rainfall anomalies are in red (blue). The contour interval is  $0.05 g kg^{-1} s^{-1}$ . For rainfall, 95% significance anomalies according to a  $t$  test are shown by a thick solid circle. For all other variables, only the 95% significance anomalies according to a  $t$  test are displayed.

*b. Global-scale MJO*

Figure 3 shows intraseasonal modulations of large-scale atmospheric convection and moisture fluxes by the MJO over the SWIO, as well as local rainfall signals over Madagascar.

The largest wet (dry) anomalies close to Madagascar are found during phase 2–3 (phases 6–7). This is fully confirmed by rain gauge records, demonstrating thus the robustness of the MJO effects at local scales. During phases 2–3, large-scale convection is already located northeast of the region of interest, and westerly anomalies prevail in the lower troposphere (Figs. 3b,c). Consequently, the northwestern part of Madagascar experiences the wettest conditions, while a few stations

in the northeast experience dry conditions. During the dry phases, signals are approximately of the opposite sign; negative rainfall anomalies tend to be of larger amplitude in the northwest, concomitant with easterly moisture flux anomalies in the lower troposphere (Figs. 3f,g). Large-scale OLR and local-scale rainfall signals are much weaker during the other phases of the MJO, and in the case of the latter, much more noisy spatially.

One may now question to what extent the regional-scale convective regimes and the global-scale MJO covary, and thus, whether the two partitionings discussed above extract redundant or distinct fractions of the whole (rainfall and climate) variability.

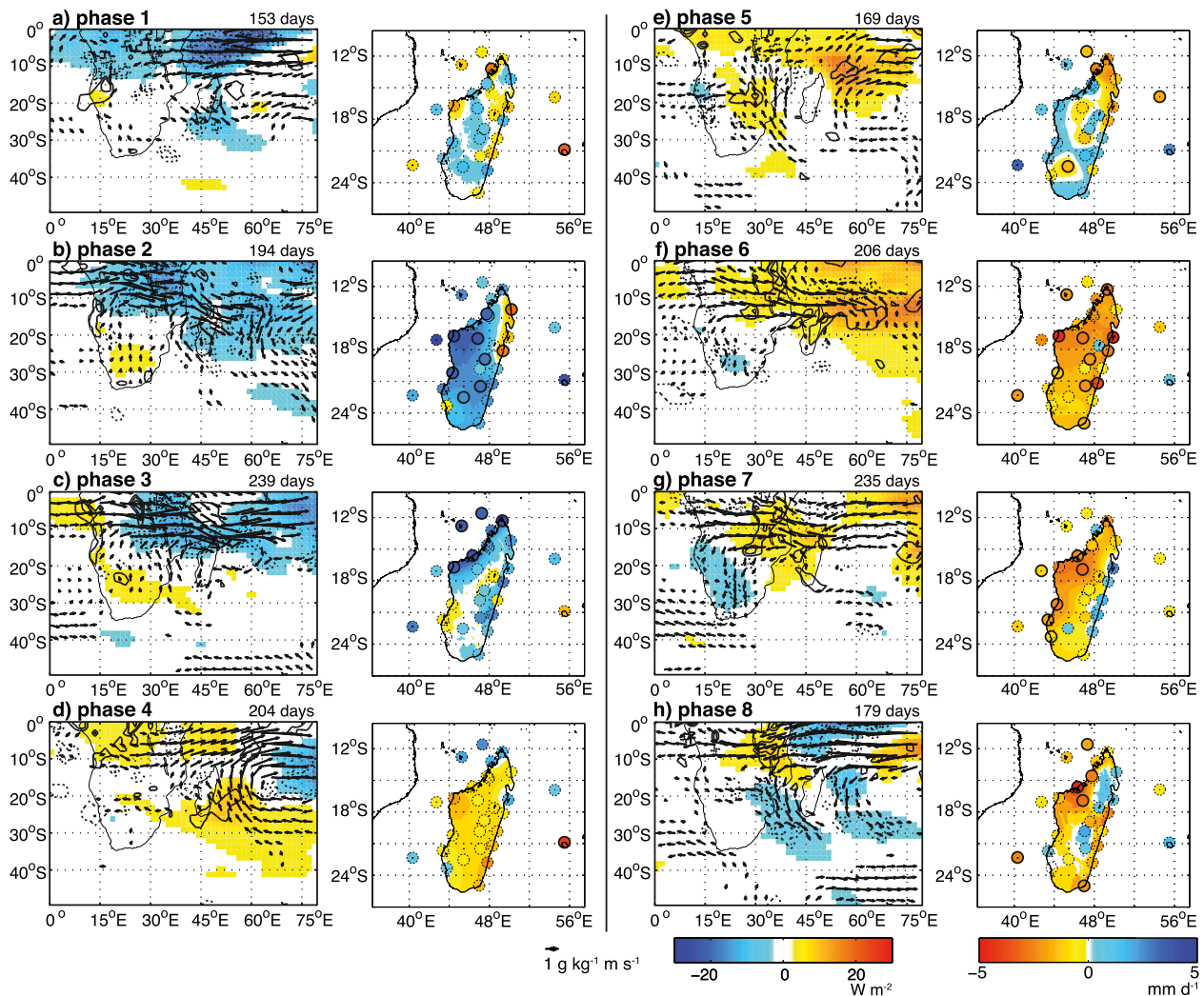


FIG. 3. As in Fig. 2, but for the eight phases of the MJO phases defined over the period NDJF from 1979 to 1999.

### c. Additively between the convective regimes and the MJO

Concomitance between phases of MJO and OLR regimes is given in Table 1. Neu's test (Neu et al. 1974) allows identifying more precisely which OLR classes and MJO phases are significantly associated (i.e., more or less frequently than the average). Regimes 1, 2, and 7 show significant associations with the phases 3, 6, and 4 of MJO, respectively. However, convective regimes are statistically independent of the global-scale MJO activity; most regimes are equiprobable throughout the MJO life cycle. This conclusion holds for TTT, hereby corroborating Pohl et al. (2009); it should, however, be noted that, more recently, Hart et al. (2013) suggest that the intensity of TTT could be weakly modulated by the MJO phase, although their occurrences are homogeneously

distributed over its phases. To quantify the fraction of regional-scale convection and local-scale rainfall variability over Madagascar explained by the regimes and the MJO, Fig. 4 shows the percentage of OLR and rainfall variance explained by the discretization into seven regimes (Fig. 4a) and nine MJO phases (including one of weak intraseasonal activity when the MJO amplitude is lesser than one standard deviation according to the RMM indices; Fig. 4b). The percentage of rainfall variance explained is first computed for each rain gauge station and is then interpolated according to the RK methodology. The additivity between the two classifications is addressed by considering all possible combinations between the regimes and the MJO (i.e.,  $7 \times 9 = 63$  classes; Fig. 4c). All daily fields (rainfall or OLR) are replaced by the average composite field during the occurrences of the corresponding regime or class (resulting

TABLE 1. Contingency table between classes of OLR and phases of MJO. Boldface values are overrepresented and the others values are underrepresented. Italics denote 95% significance according to Neu's test.

		Convective regimes							$\Sigma$
		1	2	3	4	5	6	7	
MJO phase	1	28	13	<b>31</b>	<b>18</b>	19	<b>23</b>	<b>21</b>	153
	2	25	<b>36</b>	<b>35</b>	<b>30</b>	19	21	<b>28</b>	194
	3	<b>20</b>	<b>49</b>	<b>45</b>	<b>48</b>	23	28	26	239
	4	<b>50</b>	<b>26</b>	<b>41</b>	21	<b>35</b>	20	<b>11</b>	204
	5	<b>45</b>	11	26	17	24	21	<b>25</b>	169
	6	<b>63</b>	5	28	17	<b>40</b>	<b>30</b>	23	206
	7	<b>69</b>	18	25	17	<b>44</b>	27	<b>35</b>	235
	8	25	<b>23</b>	20	11	<b>39</b>	<b>28</b>	<b>33</b>	179
	$\Sigma$	325	181	251	179	243	198	202	1579

thus in suppressing intraclass or intraregime variability); one calculates next the ratio between such reconstructed data and the raw original time series.

Results show (i) that the regimes (MJO) explain up to 25%–30% (8%–10%) of OLR variability in the central parts (very low latitudes) of the domain [especially equatorial East Africa; Pohl and Camberlin (2006)], this is not surprising since the regimes were designed to maximize regional variance over this same domain while the MJO is primarily a mode of tropical variability; (ii) that the amounts of explained rainfall variance over Madagascar only reach 2%–3% for the regimes (with a decrease from south to north) and 1%–2% for the MJO (mostly in the northwest), hereby illustrating the usefulness of in situ local observations to monitor the rainfall field against smoothed, larger-scale, satellite-derived or reanalyzed estimations; (iii) that the regimes (MJO) significantly discriminate rainfall variability over the whole island except the north (only over the northwest); and (iv) that for both fields the results seem to be additive (i.e., in agreement with Table 1 that the redundancy between the two partitionings seems to be negligible). Local-scale effects associated with land–sea contrasts, the topography (and derived variables: slope, exposition, ...), or surface properties (albedo, land-use, ...) seem to play a predominant role in local-scale rainfall. High-resolution climate modeling could help detail associated processes and mechanisms.

#### 4. Conclusions and discussion

This work investigates local-scale rainfall variability over Madagascar, and its embedment in larger-scale recurrent atmospheric configurations, as inferred by regional convective regimes on the one hand and the phases of the MJO defined over the whole tropical belt

on the other hand. To that end, 28 rain gauge records are extracted from an original database of daily rainfall data measured in situ over Madagascar, the Réunion Island, Mayotte, and the Scattered Islands.

Our results show (i) for both regimes and MJO, a general consistency between regional-scale features of Malagasy rainfall variability (e.g., longitudinal or latitudinal gradients, side oppositions) and large-scale moisture flux and/or convective configurations such as inferred from reanalyses; (ii) some local features (e.g., slopes or sea breezes) likely to produce significant rainfall anomalies that modulate the above-mentioned patterns (TTT and MJO) at fine scales; and (iii) a significant influence of TTT over Madagascar and the neighboring islands. The latter point, although consistent with large-scale fields and, therefore, rather intuitive, was not specifically discussed in previous work (e.g., Fauchereau et al. 2009; Hart et al. 2013). It could nevertheless be important for the region for operational weather prediction. Wet conditions over Madagascar prevail during occurrences of regimes 6–7 (i.e., the mature and decaying phases of TTT systems that often succeed the early stage materialized here by regime 5). On average, the occurrences of such systems over southern Africa and the Mozambique Channel can thus be seen as precursors of Malagasy wet spells, especially over the southern part of the island. (iv) Regional and local effects of the MJO are weaker on average, and only concern the northwest of Madagascar and the north of the Mozambique Channel. Additional complexity may be introduced by the diversity of large-scale MJO events themselves (Pohl and Camberlin 2014), likely to strongly modulate their effects on local rainfall.

This work is a first step to document rainfall variability at regional and local scales. The amount of variance explained by our regimes and by the MJO remains, however, rather weak (up to 30%–35% according to reanalyses, but only 6% according to rain gauge records, when both influences are combined). This suggests that local effects play a major role, and that other climate phenomena modulating regional variability, in addition to those discussed here, should be included in future analyses. Equatorial Rossby waves, for instance, could have significant effects on Malagasy rainfall by modulating TC genesis (Bessafi and Wheeler 2006). Madagascar and neighboring regions also correspond to the region where ENSO effects on rainfall change sign (seasonal dryness in southern Africa during El Niño years, contrasting with wet conditions over equatorial East Africa). The database used for this work could help document this transition at the finescale, the role of surface topography on atmospheric flows and associated anomalies, and possibly the contrasting effects of the ENSO flavors.

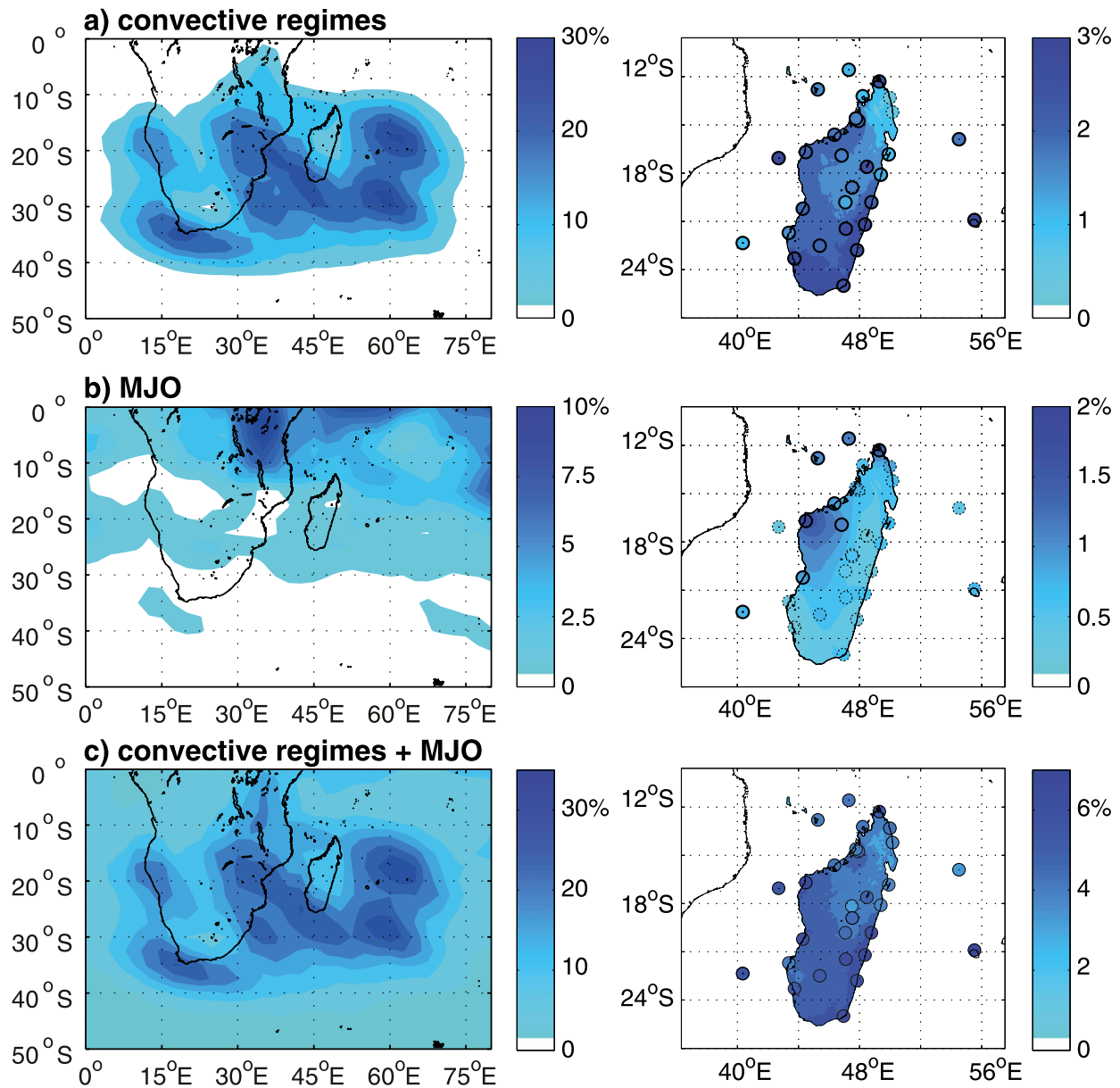


FIG. 4. (a) Percentage of (left) OLR variance and (right) daily rainfall explained by convective regimes. Stations surrounded by a solid line are significant according to the Fisher test. (b) As in (a), but for MJO. (c) As in (a), but for both convective regimes and MJO. The color scales are different for each panel for readability.

**Acknowledgments.** The authors thank two anonymous reviewers for their constructive comments. Calculations were performed using HPC resources from DSI-CCUB, Université de Bourgogne. This study is dedicated to the memory of Professor Andrianaharimanana Razafindrabe.

#### REFERENCES

- Bessafi, M., and M. C. Wheeler, 2006: Modulation of south Indian Ocean tropical cyclones by the Madden–Julian oscillation and convectively coupled equatorial waves. *Mon. Wea. Rev.*, **134**, 638–656, doi:10.1175/MWR3087.1.
- Cheng, X., and J. M. Wallace, 1993: Regime analysis of the Northern Hemisphere wintertime 500-hPa height field: Spatial patterns. *J. Atmos. Sci.*, **50**, 2674–2696, doi:10.1175/1520-0469(1993)050<2674:CAOTNH>2.0.CO;2.
- Fauchereau, N., B. Pohl, C. Reason, M. Rouault, and Y. Richard, 2009: Recurrent daily OLR patterns in the southern Africa/southwest Indian Ocean region, implications for South African rainfall and teleconnections. *Climate Dyn.*, **32**, 575–591, doi:10.1007/s00382-008-0426-2.
- Funk, C. C., and Coauthors, 2014: A quasi-global precipitation time series for drought monitoring. U.S. Geological Survey Data Series 832, 4 pp., doi:10.3133/ds832.

- Hart, N. C. G., C. J. C. Reason, and N. Fauchereau, 2013: Cloud bands over southern Africa: Seasonality, contribution to rainfall variability and modulation by the MJO. *Climate Dyn.*, **41**, 1199–1212, doi:10.1007/s00382-012-1589-4.
- Hengl, T., 2009: *A Practical Guide to Geostatistical Mapping*. University of Amsterdam, 270 pp.
- , G. B. M. Heuvelink, and D. G. Rossiter, 2007: About regression-kriging: From equations to case studies. *Comput. Geosci.*, **33**, 1301–1315, doi:10.1016/j.cageo.2007.05.001.
- Jury, M. R., B. A. Parker, N. Raholijao, and A. Nassor, 1995: Variability of summer rainfall over Madagascar: Climate determinants at interannual scales. *Int. J. Climatol.*, **15**, 1323–1332, doi:10.1002/joc.3370151203.
- Lloyd, C. D., 2010: Nonstationary models for exploring and mapping monthly precipitation in the United Kingdom. *Int. J. Climatol.*, **30**, 390–405, doi:10.1002/joc.1892.
- Macron, C., B. Pohl, Y. Richard, and M. Bessafi, 2014: How do tropical temperate troughs form and develop over southern Africa? *J. Climate*, **27**, 1633–1647, doi:10.1175/JCLI-D-13-00175.1.
- Michelangeli, P., R. Vautard, and B. Legras, 1995: Weather regime occurrence and quasi-stationarity. *J. Atmos. Sci.*, **52**, 1237–1256, doi:10.1175/1520-0469(1995)052<1237:WRRASQ>2.0.CO;2.
- Morel, B., B. Pohl, Y. Richard, B. Bois, and M. Bessafi, 2014: Regionalizing rainfall at very high resolution over La Réunion Island using a regional climate model. *Mon. Wea. Rev.*, **142**, 2665–2686, doi:10.1175/MWR-D-14-00009.1.
- Nassor, A., and M. R. Jury, 1997: Intra-seasonal climate variability of Madagascar. Part 2: Evolution of flood events. *Meteor. Atmos. Phys.*, **64**, 243–254, doi:10.1007/BF01029696.
- , and —, 1998: Intra-seasonal climate variability of Madagascar. Part 1: Mean summer conditions. *Meteor. Atmos. Phys.*, **65**, 31–41, doi:10.1007/BF01030267.
- Neu, C. W., C. R. Byers, and J. M. Peek, 1974: A technique for analysis utilization-availability data. *J. Wildl. Manage.*, **38**, 541–545, doi:10.2307/3800887.
- Odeh, I. O. A., A. B. McBratney, and D. J. Chittleborough, 1995: Further results on prediction of soil properties from terrain attributes: Heterotopic cokriging and regression-kriging. *Geoderma*, **67**, 215–226, doi:10.1016/0016-7061(95)00007-B.
- Pebesma, E. J., 2004: Multivariate geostatistics in S: The gstst package. *Comput. Geosci.*, **30**, 683–691, doi:10.1016/j.cageo.2004.03.012.
- Pohl, B., and P. Camberlin, 2006: Influence of the Madden-Julian Oscillation on East African rainfall. I: Intraseasonal variability and regional dependency. *Quart. J. Roy. Meteor. Soc.*, **132**, 2521–2539, doi:10.1256/qj.05.104.
- , and —, 2014: A typology for intraseasonal oscillations. *Int. J. Climatol.*, **34**, 430–445, doi:10.1002/joc.3696.
- , Y. Richard, and N. Fauchereau, 2007: Influence of the Madden-Julian oscillation on southern African summer rainfall. *J. Climate*, **20**, 4227–4242, doi:10.1175/JCLI4231.1.
- , N. Fauchereau, Y. Richard, M. Rouault, and C. J. C. Reason, 2009: Interactions between synoptic, intraseasonal and interannual convective variability over Southern Africa. *Climate Dyn.*, **33**, 1033–1050, doi:10.1007/s00382-008-0485-4.
- Prudhomme, C., and D. W. Reed, 1999: Mapping extreme rainfall in a mountainous region using geostatistical techniques: A case study in Scotland. *Int. J. Climatol.*, **19**, 1337–1356, doi:10.1002/(SICI)1097-0088(199910)19:12<1337::AID-JOC421>3.0.CO;2-G.
- Todd, M., and R. Washington, 1999: Circulation anomalies associated with tropical-temperate troughs in Southern Africa and the southwest Indian Ocean. *Climate Dyn.*, **15**, 937–951, doi:10.1007/s003820050323.
- Uppala, S., and Coauthors, 2005: The ERA-40 re-analysis. *Quart. J. Roy. Meteor. Soc.*, **131**, 2961–3012, doi:10.1256/qj.04.176.
- Vigaud, N., B. Pohl, and J. Crétaf, 2012: Tropical-temperate interactions over southern Africa simulated by a regional climate model. *Climate Dyn.*, **39**, 2895–2916, doi:10.1007/s00382-012-1314-3.
- Washington, R., and M. Todd, 1999: Tropical-temperate links in southern Africa and southwest Indian Ocean satellite-derived daily rainfall. *Int. J. Climatol.*, **19**, 1601–1616, doi:10.1002/(SICI)1097-0088(19991130)19:14<1601::AID-JOC407>3.0.CO;2-0.
- Wheeler, M. C., and H. H. Hendon, 2004: An all-season real-time multivariate MJO index: Development of an index for monitoring and prediction. *Mon. Wea. Rev.*, **132**, 1917–1932, doi:10.1175/1520-0493(2004)132<1917:AARMMI>2.0.CO;2.